Optimizing the Catalyst Distribution for Countercurrent Methane Steam Reforming in Plate Reactors

Monica Zanfir and Michael Baldea
Praxair Technology Center, Praxair, Inc., 150 East Park Dr, Tonawanda, NY 14150

Prodromos Daoutidis
Dept. of Chemical Engineering and Materials Science, University of Minnesota, Minneapolis, MN 55455

DOI 10.1002/aic.12474
Published online December 9, 2010 in Wiley Online Library (wileyonlinelibrary.com).

Microscale autothermal reactors remain one of the most promising technologies for efficient hydrogen generation. The typical reactor design alternates microchannels where reforming and catalytic combustion of methane occur, so that exothermic and endothermic reactions take place in close proximity. The influence of flow arrangement on the autothermal coupling of methane steam reforming and methane catalytic combustion in catalytic plate reactors is investigated. The reactor thermal behavior and performance for cocurrent and countercurrent are simulated and compared. A partial overlapping of the catalyst zones in adjacent exothermic and endothermic channels is shown to avoid both severe temperature excursions and reactor extinction. Using an innovative, optimization-based approach for determining the catalyst zone overlap, a solution is provided to the problem of determining the maximum reactor conversion within specified temperature bounds, designed to preserve reactor integrity and operational safety. © 2010 American Institute of Chemical Engineers *AIChE J*, 57: 2518–2528, 2011
Keywords: reactor analysis, mathematical modeling, optimization, numerical solutions

Introduction

Over the past half century, the chemical industry has been driven by the economy of scale. Chemical engineers built ever larger plants to increase efficiency and reduce per-unit production costs. This approach entailed, however, several disadvantages, including increased safety and environmental risks due to large inventories of hazardous materials and economic risks caused by overcapacity.

New trends in chemical engineering promote process intensification and the use of flexible, miniaturized plants that facilitate localized production.[1] Several key elements are widely accepted as drivers for future development[2]: a reduction in capital investments and energy use, increased process flexibility and lower inventories, an ever greater emphasis on process safety, and improved environmental performance. The motivation and goal behind process intensification is thus "to do more with less." In intensified processes, the transfer and transport limitations are minimized, and the process is governed by chemical reaction rates.[3] Microchemical engineering is both a direct product and a driver of process intensification and miniaturization: working on a small scale facilitates the adaptation of the equipment to the process requirements and, at the same time, the combination of multiple operations in a reduced number of physical units.

Within the realm of process intensification, microchannel process technology has made significant strides over the last decade,[4] with methane steam reforming reactors aimed at small-scale hydrogen production being one of its most

Correspondence concerning this article should be addressed to M. Zanfir at monica_zanfir@praxair.com, and M. Baldea at michael_baldea@praxair.com.

© 2010 American Institute of Chemical Engineers

suitable applications as well as one of its most notable products. Typical reactor designs alternate microchannels for reforming and catalytic combustion, so that the exothermic and endothermic reactions take place in close proximity. These channels typically have a height of the order of millimeters and a catalyst thickness of the order of microns. The advantages of microreactors over conventional reactors are the high heat transfer coefficients and minimal intracatalyst diffusion resistance,[1,5] which leads to an order-of-magnitude reduction in reactor size.[6] Novel manufacturing techniques[7–9] have recently allowed microchannel technology to materialize in commercial offerings such as a gas-to-liquids process.[10]

Despite these advances, several design challenges must be overcome. Most studies and applications favor a cocurrent design, whereby the reforming mixture and the fuel are fed at the same end of the reactor. A countercurrent layout would bring the advantage of a greatly simplified flow distribution and reactor assembly. However, producing balanced countercurrent designs that match the rates of heat generation in the exothermic channels and heat consumption in the endothermic channels remains an important issue.[11–15] Previous studies[11,13,15] indicate that the coupling of methane steam reforming with methane combustion in a countercurrent flow arrangement is difficult: the reactant depletion occurs in opposite directions relative to the reactor length. This complicates the efficient synchronization of the reaction rates and therefore the rate of heat generation and heat consumption, with the reactor thermal behavior typically drifting to one of two extremes:

- if the heat generated in the combustion side cannot be consumed at the same rate, the temperature increases beyond acceptable limits, resulting in hot spots that can destroy the catalyst coating and jeopardize the structural integrity of the supporting material.
- if the endothermic reaction rates are higher than the combustion reaction rates, the temperature drops, resulting in reactor extinction.

The effective countercurrent coupling of exothermic and endothermic reactions and, equivalently, improving the match between the respective heat generation and heat consumption rates require modifications to the reactor design.[16] Alternatives include using a distributed fuel feed along the reactor length (rather than feeding all the fuel flow at one end), multiple passes for better heat recovery,[5] and a setup that features a shifted, incomplete overlap of the catalyst-coated zones in the combustion and reforming channels. Modifying the activity of the catalyst is a further option for alleviating issues related to the formation of hotspots,[17] shown to be effective in cocurrent setups but bringing limited benefits to countercurrent designs.[18]

This article investigates the influence of flow arrangement and catalyst distribution for autothermal coupling of methane steam reforming and methane catalytic combustion in catalytic plate reactors. The reactor thermal behavior and performance for cocurrent and countercurrent flow are simulated and compared. A design involving a partial overlap of the catalyst zones in adjacent exothermic and endothermic channels is proposed to avoid both severe temperature excursions and the extinction of the reactor. A novel, rigorous optimization-based approach for determining the catalyst zone overlap that results in a maximum reactor conversion within specified temperature bounds is introduced. Using the dynamic model of the reactor, a time relaxation-based solution technique is presented for the optimization problem. Several model modifications, which exploit the physical characteristics of the reactor model to improve its numerical solution properties without altering the steady-state solution, are also presented.

Description of the Reaction System

The reaction system considered in this work is the endothermic steam reforming of methane and methane catalytic and homogeneous combustion, taking place in alternate channels of a catalytic plate reactor (CPR). The main chemical reactions involved in the reforming process are

- methane steam reforming $\quad CH_4 + H_2O \Leftrightarrow CO + 3H_2$

$$\Delta H = +206.1\ \text{kJ mol}^{-1} \quad (1)$$

- water−gas−shift $\quad CO + H_2O \Leftrightarrow CO_2 + H_2$

$$\Delta H = -41\ \text{kJ mol}^{-1} \quad (2)$$

- reverse methanation $\quad CH_4 + 2H_2O \Leftrightarrow CO_2 + 4H_2$

$$\Delta H = +164\ \text{kJ mol}^{-1} \quad (3)$$

Side reactions may involve carbon deposition that can be suppressed by using an excess of steam at minimum molar ratio steam:methane of 1.7. However, in a conventional steam methane reformer, a steam to carbon ration of 2.8 is most commonly used. A study by Elnashaie et al.[19] showed that the general rate equation based on Langmuir-Hinshelwood-Hougen-Watson approach, developed by Xu and Froment[20] for a 15.2% $Ni/MgAl_2O_3$ catalyst, describes most accurately the process for a wide range of parameters. Consequently, this kinetics is used in this work to describe the steam reforming process. The rate equations for the chemical reactions (1), (2), and (3) are

$$r_1 = \frac{\frac{k_1}{p_{H_2}^{2.5}}\left(p_{CH_4}\cdot p_{H_2O} - \frac{p_{H_2}^3 \cdot p_{CO}}{K_{e,1}}\right)}{(\text{Den})^2}, \quad \text{kmol kg}_{\text{cat}}^{-1}\ \text{h}^{-1} \quad (4)$$

$$r_2 = \frac{\frac{k_2}{p_{H_2}}\left(p_{CO}\cdot p_{H_2O} - \frac{p_{H_2}\cdot p_{CO_2}}{K_{e,2}}\right)}{(\text{Den})^2}, \quad \text{kmol kg}_{\text{cat}}^{-1}\ \text{h}^{-1} \quad (5)$$

$$r_3 = \frac{\frac{k_3}{p_{H_2}^{3.5}}\left(p_{CH_4}\cdot p_{H_2O}^2 - \frac{p_{H_2}^4 \cdot p_{CO_2}}{K_{e,3}}\right)}{(\text{Den})^2}, \quad \text{kmol kg}_{\text{cat}}^{-1}\ \text{h}^{-1} \quad (6)$$

where:

$$\text{Den} = 1 + K_{CO}p_{CO} + K_{H_2}p_{H_2} + K_{CH_4}p_{CH_4} + K_{H_2O}p_{H_2O}/p_{H_2} \quad (7)$$

The values of pre-exponential factors, activation energies, heats of adsorption, and equilibrium constants are given in Table 1.

Catalytic combustion of methane is most commonly carried out by supported noble metal catalysts (Pt, Pd, and Rh).

Table 1. Pre-Exponential Factors for Reaction Rates, Heats of Adsorption, and Corresponding Activation Energies

Constant	Pre-Exponential Factor $A(k_k)$; $A(K_i)$	Activation Energy, E_k (kJ mol^{-1}), Heat of Adsorption $(-\Delta H)_k$ (kJ mol^{-1})
k_1 (kmol bar$^{0.5}$ kg$_{cat}^{-1}$ h^{-1})	4.225×10^{15}	240.1
k_2 (kmol kg$_{cat}^{-1}$ h^{-1} bar^{-1})	1.955×10^{6}	67.13
k_3 (kmol bar$^{0.5}$ kg$_{cat}^{-1}$ h^{-1})	1.020×10^{15}	243.9
K_{CO} (bar^{-1})	8.23×10^{-5}	70.65
K_{CH_4} (bar^{-1})	6.65×10^{-4}	38.28
K_{H_20}	1.77×10^{5}	−88.68
K_{H_2} (bar^{-1})	6.12×10^{-9}	82.9
$K_{e,1} = \exp(-26{,}830/T + 30.114)$ (bar^2)		
$K_{e,2} = \exp(4400/T - 4.036)$		
$K_{e,3} = \exp(-22{,}430/T + 26.078)$ (bar^2)		

The last three lines give equilibrium constants for steam reforming, water–gas shift, and reverse methanation.

With both Pd and Pt catalysts, the reaction order in oxygen tends toward zero, while the order in methane is usually about unity. The activation energy depends on the metal and reaction conditions. For methane catalytic combustion, the activation energies were found to have values in the range of 75–200 kJ mol^{-1}.[21–26] In this work, a first-order kinetic expression with respect to methane was used in the calculations along with activation energy of 90 kJ mol^{-1}. Homogeneous combustion has a contribution at high temperature. The reaction order related to methane and oxygen for homogeneous combustion is −0.3 and 1.3, respectively, with a pre-exponential factor of 8.3×10^5 s^{-1} and activation energy of 125.49 kJ mol^{-1}.[27]

Mathematical Model

A two-dimensional (2-D) dynamic reactor model has been developed to investigate the influence of flow arrangement for a catalytic plate reactor. The model considers a single plate within the reactor, together with the adjacent channels that accommodate the catalyst layers, as represented in Figure 1. Symmetry boundary conditions are imposed at the centerlines of the channels. A 2-D geometry was adopted for the gas phase and the solid wall. The catalyst layers were modeled using a 1-D approach, justified by the fact that their thickness is small compared with the reactor length (the aspect ratio $\frac{\delta^{cat}}{L} \approx 6.7 \cdot 10^{-5}$).

The inlet velocity profile considered was that of a fully developed laminar flow between two infinite parallel plates,[28] with the Reynolds number ranging between 50 and 300 for the calculations performed. The velocity variation in the reactor takes into account the influence of temperature and composition changes so that the global mass balance is satisfied

$$\int_0^{R_j} \rho_j u_{z_j} dx_j \Big|_{z=0} = \int_0^{R_j} \rho_j u_{z_j} dx_j \Big|_{\forall z} \tag{8}$$

The temperature dependence of the physical properties of the chemical species was also incorporated.[6] The diffusion coefficients were calculated assuming a binary mixture between component i and H_2O (reforming channel) or air (combustion channel). The effective diffusion coefficient for the catalyst layer is calculated from

$$D_{\mathrm{eff}_{i,j}} = \frac{\varepsilon}{\tau} \cdot \left(\frac{1}{D_{K_{i,j}}} + \frac{1}{D_{Gi,j}} \right)^{-1} \tag{9}$$

where $D_{G_{i,j}}$ is molecular diffusion coefficient calculated by Fuller's method and the Knudsen diffusion coefficient, and $D_{K_{i,j}}$ is calculated[29] as

$$D_{K_{i,j}} = 97 R_p \sqrt{\frac{T_j^{cat}}{M_{i,j}}} \tag{10}$$

The mathematical formulation of the CPR model is given in Table 2. It consists of mass balances for all the species in the gas phase and the catalyst layers and heat balances for both the reforming and the combustion channel, as well as the solid wall.

The performance of the reactor is evaluated in terms of conversion, which is calculated by integrating the local mass flow rate in each channel

$$X_j(z) = 1 - \frac{\int_0^{R_j} \rho_j u_{z_j} \omega_{CH_{4,j}} dx_j \Big|_z}{\int_0^{R_j} \rho_j u_{z_j} \omega_{CH_{4,j}} dx_j \Big|_{z=0}} \tag{11}$$

where $\omega_{CH_{4,j}}$ is the mass fraction of methane.

Numerical Solution

The mathematical model was implemented and solved in gPROMS.[30] A backward finite difference method of the second order was used for discretizing the spatial partial derivatives over 40 nodes along the axial direction, whereas orthogonal collocation on finite elements was used for the transverse direction. The latter choice was motivated by the predominantly dispersive nature of the transverse mass and heat transport.[31] Third-order polynomials over three finite elements were used.

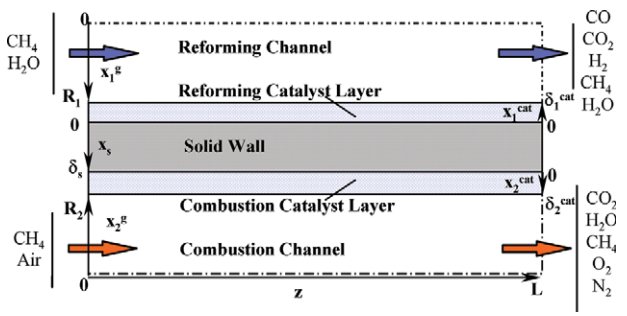

Figure 1. Single-plate geometry within the catalytic plate reactor depicting the modeling domains.

Full-length catalyst distribution. [Color figure can be viewed in the online issue, which is available at wileyonlinelibrary.com.]

Table 2. Mathematical Model

Gas Phase

Mass balances

$$\frac{\partial \rho_j}{\partial t} + \rho_j u_{z_j} \frac{\partial \omega^g_{i,j}}{\partial z} = \frac{\partial}{\partial x^g_j}\left(\rho_j D_{i-\mathrm{mix}_j} \frac{\partial \omega^g_{i,j}}{\partial x^g_j}\right) + \frac{\partial}{\partial z}\left(\rho_j D_{i_j-\mathrm{mix}_j} \frac{\partial \omega^g_{i,j}}{\partial z}\right) + \sum_k \left(v_{i,k,j} \cdot r_{\mathrm{homog}\cdot k,j} \cdot M_{i,j}\right)$$

Energy balances

$$\rho_j c_{pj} \frac{\partial T^g_j}{\partial t} + \rho_j u_{z_j} c_{pj} \frac{\partial T^g_j}{\partial z} = \frac{\partial}{\partial x^g_j}\left(k_j \frac{\partial T^g_j}{\partial x^g_j}\right) + \frac{\partial}{\partial z}\left(k_j \frac{\partial T^g_j}{\partial z}\right)$$

Continuity equation

$$\frac{\partial \rho_j}{\partial t} + \frac{\partial \rho_j u_{z_j}}{\partial z} = 0$$

Equation of state for ideal gas

$$\rho_j = \frac{P_j}{R_g T^g_j} \cdot \left(\sum_i \frac{\omega^g_{i,j}}{M_{i,j}}\right)^{-1}$$

Boundary conditions

1. Inlet conditions:
   For co-current flow:
   $z = 0; \quad \forall x^g_j$ for channels 1 and 2
   For countercurrent flow:
   $z = 0; \quad \forall x^g_j$ for channel 1 (reforming process)
   $z = L; \quad \forall x^g_j$ for channel 2 (combustion process)
   - inlet composition: $\omega^g_{i,j} = \omega^0_{i,j}$
   - inlet temperature: $T^g_j = T^0_j$
   - parabolic inlet velocity profile $u_{z_j} = 1.5 \cdot u^0_{z_j}\left[1 - \left(\frac{x^g_j}{R_j}\right)^2\right]$
2. Outlet conditions:
   For cocurrent flow:
   $z = L; \quad \forall x^g_j$ for channels 1 and 2
   For countercurrent flow:
   $z = L; \quad \forall x^g_j$ for channel 1 (reforming process)
   $z = 0; \quad \forall x^g_j$ for channel 2 (combustion process)
   - zero flux $\frac{\partial \omega^g_{i,j}}{\partial z} = \frac{\partial T^g_j}{\partial z} = \frac{\partial u_{z_j}}{\partial z} = 0$
3. Channel center: $\forall z; \quad x^g_j = 0$
   - symmetry $\frac{\partial \omega^g_{i,j}}{\partial x^g_j} = \frac{\partial T^g_j}{\partial x^g_j} = \frac{\partial u_{z_j}}{\partial x^g_j} = 0$
4. Catalyst surface conditions: $\forall z; \quad x^g_j = R_j$

$$\rho_j D_{G,i-\mathrm{mix}_j} \left.\frac{\partial \omega^g_{i,j}}{\partial x^g_j}\right|_{x^g_j = R_1} = -\rho_j D_{\mathrm{eff\_i,j}} \left.\frac{\partial \omega^{\mathrm{cat}}_{i,j}}{\partial x^{\mathrm{cat}}_j}\right|_{x^{\mathrm{cat}}_j = \delta^{\mathrm{cat}}}$$

$$j = 1, \; k_1 \left.\frac{\partial T^g_1}{\partial x^g_1}\right|_{x^g_1 = R_1} = H_1 + \lambda_s \left.\frac{\partial T_s}{\partial x_s}\right|_{x_s = 0}$$

$$j = 2, \; k_2 \left.\frac{\partial T^g_2}{\partial x^g_2}\right|_{x_2 = R_2} = H_2 - \lambda_s \left.\frac{\partial T_s}{\partial x_s}\right|_{x_s = \delta}$$

   - no slip conditions $u_{z_j} = 0$

Catalyst Layer

Isothermal in transverse direction $T^{\mathrm{cat}}_j = \left.T^g_j\right|_{x^g_j = R_j}$

Mass balance

$$\frac{\partial}{\partial x^{\mathrm{cat}}_j}\left(\rho_j D_{\mathrm{eff\_i,j}} \frac{\partial \omega^{\mathrm{cat}}_{i,j}}{\partial x^{\mathrm{cat}}_j}\right) = -\sum_k \left(v_{i,k,j} \cdot r_{k,j} \cdot M_{i,j}\right)$$

Table 2. (Continued)

Boundary conditions

1. Inlet conditions: $z = 0; \quad \forall x^{\mathrm{cat}}_j$
   - zero flux $\frac{\partial \omega^{\mathrm{cat}}_{i,j}}{\partial z} = 0$
2. Outlet conditions: $z = L; \quad \forall x^{\mathrm{cat}}_j$
   - zero flux $\frac{\partial \omega^{\mathrm{cat}}_{i,j}}{\partial z} = 0$
3. Wall conditions: $\forall z; \quad x^{\mathrm{cat}}_j = 0$
   - zero flux $\frac{\partial \omega^{\mathrm{cat}}_{i,j}}{\partial x^{\mathrm{cat}}_j} = 0$
4. Catalyst surface conditions: $\forall z; \quad x^{\mathrm{cat}}_j = \delta^{\mathrm{cat}}$

$$\left.\omega^g_{i,j}\right|_{x^g_j = R_j} = \left.\omega^{\mathrm{cat}}_{i,j}\right|_{x^{\mathrm{cat}}_j = \delta^{\mathrm{cat}}}$$

Effectiveness factor

$$\eta_{\mathrm{eff\_k,j}} = \frac{\frac{1}{\delta^{\mathrm{cat}}} \cdot \int_0^{\delta^{\mathrm{cat}}} r_{k,j} dx^{\mathrm{cat}}_j}{\left.r_{k,j}\right|_{x^{\mathrm{cat}}_j = \delta^{\mathrm{cat}}}}$$

Reaction heat flux $H_j = \sum_k \left(-\Delta H_{k,j} \cdot \int_0^{\delta^{\mathrm{cat}}} r_{k,j} dx^{\mathrm{cat}}_j\right)$

Solid Wall

Laplace equation $\frac{\partial^2 T_s}{\partial z^2} + \frac{\partial^2 T_s}{\partial x_s^2} = 0$

Boundary conditions:

1. Inlet condition $z = 0; \quad \forall x_s; \quad \frac{\partial T_s}{\partial z} = 0$
2. Outlet condition $z = L; \quad \forall x_s; \quad \frac{\partial T_s}{\partial z} = 0$
3. Reforming wall $\forall z; \quad \left.T_s\right|_{x_s = 0} = \left.T_1\right|_{x_1 = R_1}$
4. Combustion wall $\forall z; \quad \left.T_s\right|_{x_s = \delta_s} = \left.T_2\right|_{x_2 = R_2}$

Steady-state solution

The exponential temperature dependence of the reaction rates, along with the large pre-exponential constant of the combustion reaction, led to the presence of terms of vastly different magnitudes in the model equations—even when these are written in dimensionless form—reflected in steep axial temperature and composition gradients. These traits, along with the difficulty of finding an appropriate initial guess, significantly complicate the derivation of a steady state solution for the model equations.

To mitigate these numerical challenges, a time relaxation solution approach is introduced, predicated on exploiting the dynamic component of the models for obtaining a steady-state solution. In this context, the temperatures and composition variables are considered as states of the dynamic model, which is then integrated numerically from an initial condition (rather than solving from an initial guess) until a steady state is reached (as indicated by a zero value of the time derivatives of the state variables).

Based on physical insights, the following model-level modifications were implemented:

(a) Time scale stretching: Autothermal reactors feature a multiple time scale dynamic behavior, with the transient evolution of the variables in the fluid phases being much faster

than that of the corresponding variables in the solid wall. The temperature and composition of the fluid phase are thus almost always at a quasi-steady state with respect to their solid counterparts. This discrepancy can be traced to the vast difference between the physical properties—notably density and heat capacity—of the solid and fluid phase,[13] i.e.

$$\frac{\rho_g C_{p_g}}{\rho_s C_{p_s}} << 1 \tag{12}$$

To reflect this trait, the material and energy balance equations of the fluid phase in the channels are rewritten in a stretched time scale $\tau = t/\varepsilon$

$$\frac{\partial \rho_j}{\partial \tau} = \varepsilon \frac{\partial \rho_j}{\partial t} \quad \text{and} \quad \frac{\partial T_j^g}{\partial \tau} = \varepsilon \frac{\partial T_j^g}{\partial t} \tag{13}$$

A value of $\varepsilon = 1/10{,}000$ was chosen, which is of the order of magnitude of the above heat capacity-density ratio.

This results in "speeding up" the dynamics of the fluid phase, bringing the fluid temperature and composition to a quasi-steady state. Note that this approach is practically equivalent for solving a differential-algebraic equation (DAE) system having the wall temperatures and compositions as the only differential variables. However, the numerical issues typically associated with computing consistent initial values for the algebraic variables of a DAE system[32] are eliminated.

(b) Dynamic extension: To alleviate the impact of axial stiffness on solver stability and performance, a dynamic extension is introduced, whereby the reaction rate laws are modified to include the state α

$$r_i' = \min(\alpha, 1) r_i \tag{14}$$

with

$$d\alpha/dt = \omega, \quad \alpha(t = 0) = 0 \tag{15}$$

This technique allows for the reaction rates to be increased gradually in a simulation, following a ramp profile, with significant numerical benefits. The value of ω ($\omega = 10^{-3}$) was chosen to be of the order of magnitude of the slowest natural time constant of the reactor, namely that of the wall temperature.

It is easy to verify that these modifications do not alter the steady-state problem formulation and its solution. Nevertheless, it is important to note that the transient part of the solution is distorted by the system modifications; the time-dependent temperature and composition trajectories thus obtained are not physically meaningful.

Optimization

The solution of an optimization problem entails finding the maximum (or minimum) of an objective function, $J(x,l)$, by varying a set of decision variables, l, subject to constraints, which can be expressed as either equalities (f) or inequalities (g)

$$\begin{aligned} &\max_l J(x,l) \\ &\text{s.t. } f(x,l) = 0 \\ &\quad g(x,l) \le 0 \end{aligned} \tag{16}$$

The above equation describes the most general formulation, a nonlinear program, in which both the objective and the constraints are nonlinear functions; conversely, a problem involving a linear objective and linear constraints is referred to as a linear program. The time dependence of x (and implicitly, of J,l,f) affords a further classification into steady-state (if they are time independent) and dynamic (time dependent) programs. In the dynamic case, the constraints can in turn be interior (which apply to an interval covering some or all of the period of time considered in the optimization) or end point, applied only at the end of the time period. Further details on optimization can be found in standard texts.[33,34]

As with most equipment designs, the formulation of the optimization problem for autothermal reactors entails maximizing a performance criterion (e.g., the conversion in the reforming and/or combustion channels), subject to satisfying constraints pertaining to the process, catalyst and reactor material (which will be discussed later in the article), as well as the model equations.

It is intuitive that the numerical challenges encountered in solving the model equations at steady state translate into difficulties in satisfying the corresponding constraints in a steady-state optimization scenario. To mitigate this issue, the time-relaxation strategy for obtaining a steady-state solution was extended to solving the steady-state optimization problem. Specifically, the steady-state optimization problem is formulated as a dynamic program, seeking to maximize the objective function and satisfy all the constraints at the end of the time horizon of the problem (which is chosen to be sufficiently long to allow for the reactor to reach a steady state) and ignoring the constraints as the system transitions toward steady state.

A schematic representation of the optimization algorithm is presented in Figure 2. This optimization algorithm has recently been made commercially available as part of gPROMS.[35]

Results and Discussion

Reactor performance for cocurrent flow arrangement

The thermal behavior of the cocurrent CPR—using the parameters in Table 3—has been investigated extensively in a previous study.[6] Cocurrent flow provides a good balance between the rates of heat generation (in the combustion channel) and heat consumption in the endothermic channel. Because in this case the resistance to heat transfer is minimized,[2] the heat balance depends mainly on the relationship between the rates of the endothermic and exothermic reactions. A cocurrent flow arrangement has the advantage of matching the rates at which reactants in both channels are depleted along the reactor length. As illustrated in Figure 3, the axial evolution of the methane conversion in the two channels is well synchronized, and the axial temperature profile exhibits a steady increase from the inlet to the outlet. Figure 3 shows the dimensionless transversal mid-point temperature of the metallic plate, which varies from the initial

Table 3. Data Used for Base Case Calculations

Gas Phase	Reforming Side	Combustion Side
Inlet conditions		
Composition (vol %)	21.28% CH_4 71.45% H_2O 1.19% CO_2 2.60% H_2 3.48% N_2	9.1% CH_4 90.9% Air
Temperature	793 K	
Pressure	1.1 bar	
Velocity	4 m s^{-1}	3.2 m s^{-1}
Geometry		
Plate length	0.3 m	
Channel half height	1 mm	
Catalyst layer		
Thickness	20 μm	
Pore radius	10 nm	
Porosity	0.4	
Tortuosity	4	
Thermal conductivity	0.4 W mK^{-1}	
Kinetics		
Pre-exponential factor	See Table 1	4×10^8 s^{-1}
Activation energy	See Table 1	90,000 J mol^{-1}
Solid wall		
Thickness	0.5 mm	
Thermal conductivity	25 W m^{-1} K^{-1}	

value of 1 to a maximum of 1.33 (equivalently, the temperature of the plate mid-point varies from 793 to about 1058 K). This allows high outlet conversions (95 and 98%, respectively) for both methane steam reforming and catalytic combustion. Synergistic coupling of heat generation and heat consumption is also evinced by the evolution of the axial heat fluxes, as shown in Figure 4: the peak of heat generation by combustion and heat consumption in the endothermic channel are located at almost the same axial coordinate.

Reactor performance for countercurrent flow arrangement and full-length catalyst distribution

The reactor behavior has been simulated with identical inlet conditions (Table 3) for a countercurrent flow arrangement. A full-length catalyst distribution was considered in both channels, and (as in the aforementioned cocurrent case) it was initially assumed that only catalytic combustion takes place in the combustion channel. Simulation results for the dimensionless mid-point plate temperature and for the methane conversion in both the reforming and the combustion channels are given in Figure 5. The plots indicate that a simple reversal of the flow direction results in very poor reactor performance, which can be traced to a strong mismatch in the endothermic and exothermic heat fluxes.

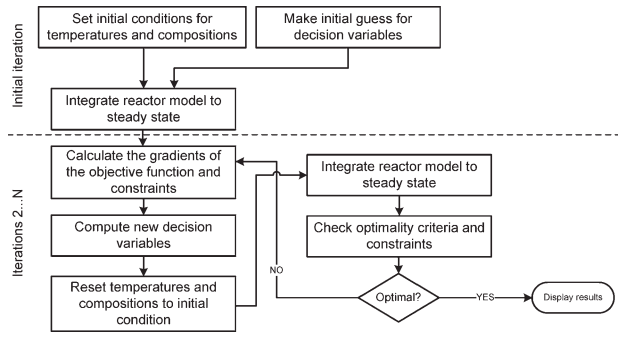

Figure 2. Optimization algorithm.

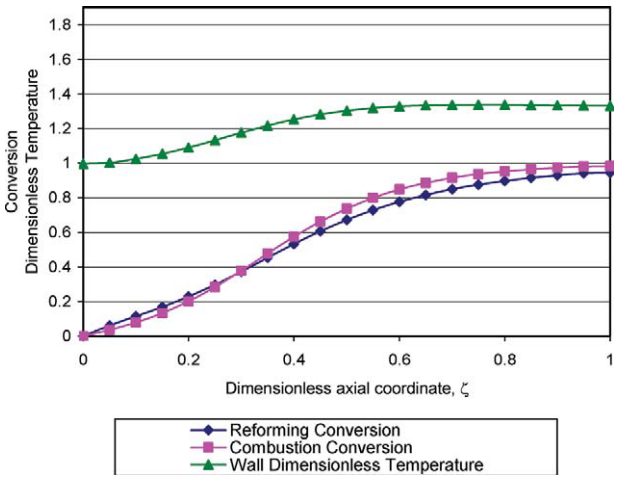

Figure 3. Evolution of combustion and reforming conversions, and the dimensionless temperature in the middle of the metallic plate along the reactor for cocurrent flow arrangement.

[Color figure can be viewed in the online issue, which is available at wileyonlinelibrary.com.]

In this case, in the combustion channel, about 70% of methane combustion conversion occurs in the first 10% of the channel length. The conversion at the outlet of the reforming channel reaches only 62%. This is mainly due to an abrupt increase close to the channel exit (which corresponds to the inlet of the combustion channel), as it is evident that almost no reactions occur within the remaining (or about 80% of the total) channel length. Clearly, the heat released cannot be efficiently transferred to support the endothermic process.

This assertion is further supported by the axial profile of the heat fluxes (Figure 6): the maximum combustion heat

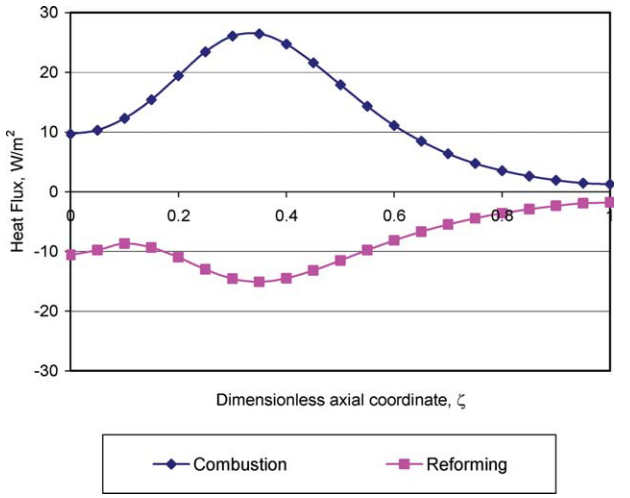

Figure 4. Evolution of exothermic and endothermic heat fluxes along the reactor for cocurrent flow arrangement.

[Color figure can be viewed in the online issue, which is available at wileyonlinelibrary.com.]

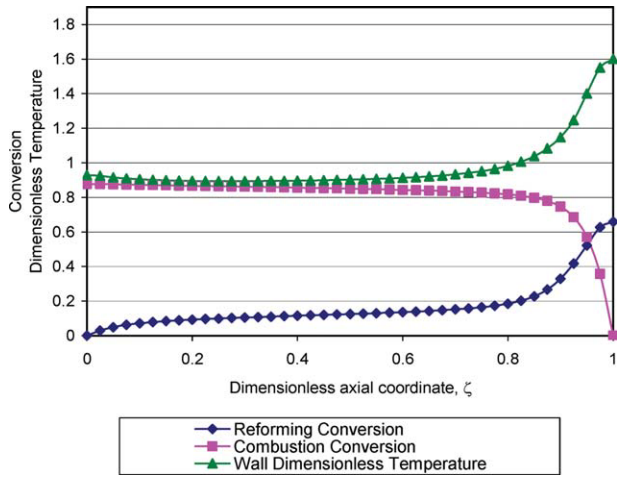

Figure 5. Evolution of combustion and reforming conversions, and the dimensionless temperature in the middle of the metallic plate along the reactor for countercurrent flow arrangement and full-length catalyst distribution.

[Color figure can be viewed in the online issue, which is available at wileyonlinelibrary.com.]

flux occurs close to the inlet of the combustion channel. From a heat transfer point of view, most of the remaining reactor length is unutilized, showing close to zero heat fluxes. Because of the inability of the endothermic process to receive the heat generated by combustion, the heat released by combustion contributes chiefly to the (inefficient) increase of the reactor temperature. Consequently, the plate mid-point temperature exhibits a much higher (1270 vs. 1058 K) maximum than in the case of cocurrent flow.

Reactor performance for countercurrent flow arrangement and optimal catalyst distribution

Previous studies and the developments presented thus far indicate that a rearrangement of the overlap of the catalyst zones in the adjacent channels is required to maximize countercurrent operation performance. A stepwise distribution, as shown in Figure 7, constitutes a natural (and practically implementable) approach. In Figure 7, the lengths L_{ref} and L_{comb} represent the distance from the reforming and combustion channel inlet to the location where the catalyst coating coverage begins in each channel. Intuitively, the choice of reactor length, L, as well as the catalyst distribution (driven by L_{ref} and L_{comb}) are critical for the performance of the reactor.[16,36] This, in turn, makes these parameters an ideal choice of decision variables in the formulation of a design optimization problem. For the autothermal reactor, the optimization problem (16) thus takes the form

$$\begin{aligned} &\max_{L_{\text{comb}},L_{\text{ref}},L} \left(X_{\text{CH}_4,\text{ref}}(L,t_{\text{final}}) + X_{\text{CH}_4,\text{comb}}(0,t_{\text{final}})\right) \\ &\text{s.t.} 1000\,\text{K} < T_{\text{wall}}(z,t_{\text{final}}) < 1500\,\text{K} \\ &\quad L < L_{\max} = 0.6\,\text{m} \\ &\quad 0 < L_{\text{ref}} < 1 \\ &\quad 0 < L_{\text{comb}} < 1 \end{aligned} \tag{17}$$

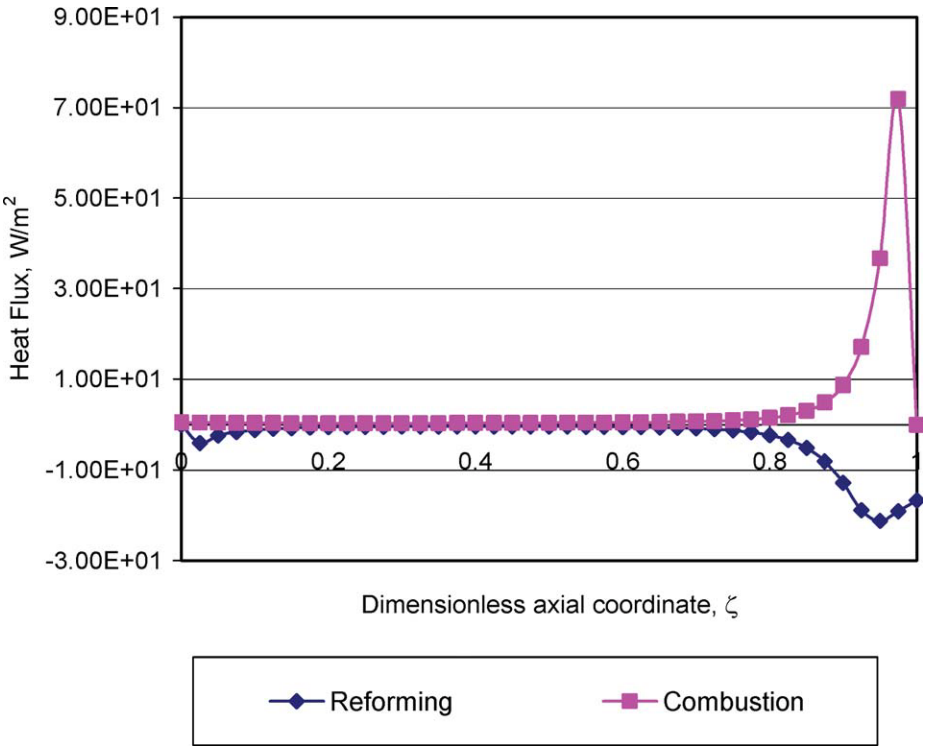

Figure 6. Evolution of exothermic and endothermic heat fluxes along the reactor for countercurrent flow arrangement and full-length catalyst distribution.

[Color figure can be viewed in the online issue, which is available at wileyonlinelibrary.com.]

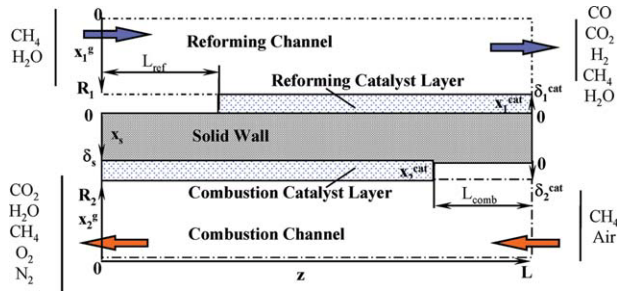

Figure 7. Single-plate geometry within the catalytic plate reactor for step size catalyst distribution.

[Color figure can be viewed in the online issue, which is available at wileyonlinelibrary.com.]

Specifically, we are interested in maximizing the sum of the values of the methane conversion at the outlets of the reforming and combustion channels, subject to maintaining the temperature above 1000 K (to prevent reactor extinction) and a maximum set at 1500 K. Naturally, the formulation above assumes that the dynamic model equations (with the modifications mentioned before) are satisfied at all times. It is important to note that the formulation in Eq. 17 can be extended to accommodate other bounds for the constraints and decision variables as well as additional constraints or decision variables (if needed); the framework we propose is completely flexible in this regard.

The optimization problem (17) was initially solved considering the same inlet conditions as in the cocurrent case and only catalytic combustion in the exothermic channel, i.e., the data in Table 3.

The solution resulted in a catalyst distribution that ensures a high reforming conversion for a maximum plate mid-point

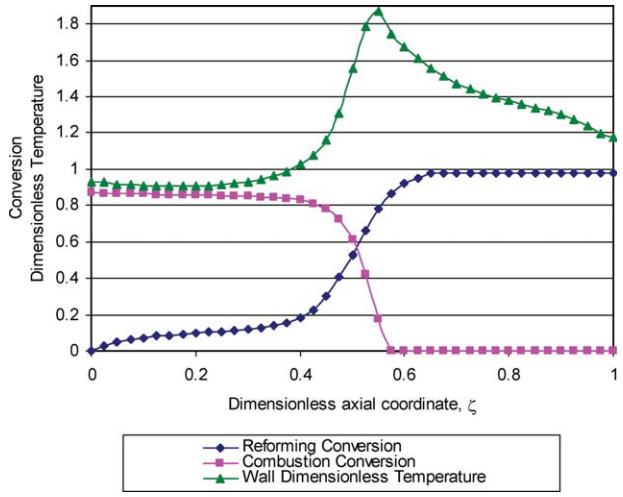

Figure 8. Evolution of combustion and reforming conversions, and the dimensionless temperature in the middle of the metallic plate along the reactor for countercurrent flow arrangement and step catalyst distribution (only catalytic combustion).

[Color figure can be viewed in the online issue, which is available at wileyonlinelibrary.com.]

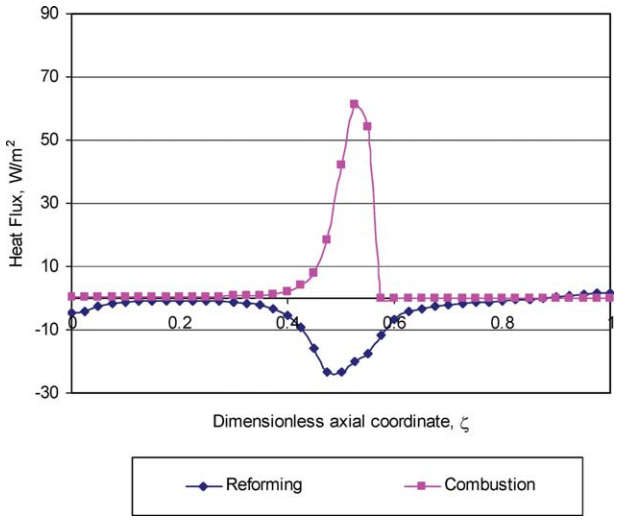

Figure 9. Evolution of exothermic and endothermic heat fluxes along the reactor for countercurrent flow arrangement and optimum step size catalyst distribution (only catalytic combustion).

[Color figure can be viewed in the online issue, which is available at wileyonlinelibrary.com.]

temperature, $T_{max} = 1484$ K. In the optimized geometry, $L = 0.6$ m, $L_{ref} = 0.0135$ m, while $L_{comb} = 0.2652$ m. The reactor profiles with optimal catalyst distribution are shown in Figure 8. It can be seen that a reforming conversion of 99% is achieved at the endothermic channel exit. The temperature maximum in the reactor occurs near the beginning of the combustion catalyst layer, which corresponds to the maximum in the heat flux generated by combustion (Figure 9). Recall that the peak of heat generation occurs at the outlet of the reforming channel for a full-length catalyst distribution. Shifting the location of the heat generation peak thus allows the generated heat to be carried downstream the reforming channel to better assist the endothermic process, improving the synchronization between the rates of heat generation and heat consumption in the two channels.

The results also indicate that operating the reactor in countercurrent flow is challenging when the operating parameters used in the cocurrent case are preserved. Although a very high reforming conversion is possible, the conversion of the fuel remains lower than in the cocurrent case, at 86.9%.

It was found that the solution of the problem is dependent on the initial guesses considered for the variables L, L_{ref}, and L_{comb}. Specifically, the high nonlinearity of the reactor model increases makes this design problem susceptible to local maxima. To account for this, the calculations were run with several initial guesses; the data reported above and in the subsequent section reflect the best results obtained in each set of calculations.

Influence of homogeneous combustion for countercurrent flow arrangement and optimal catalyst distribution

The temperature profile in Figure 8 exhibits a sharp increase at the beginning of the combustion catalyst layer;

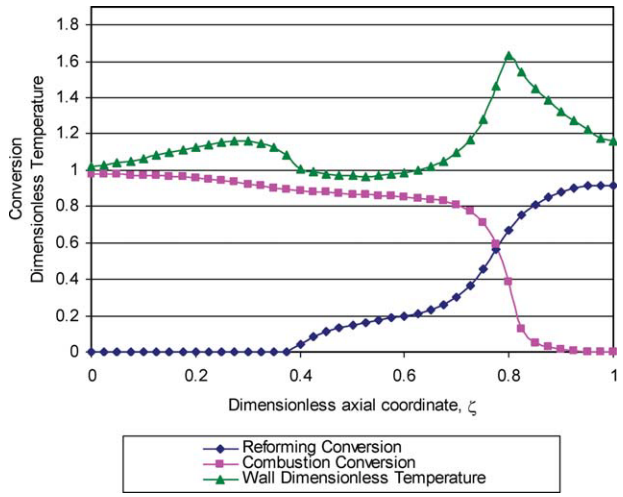

Figure 10. Evolution of combustion and reforming conversions, and the dimensionless temperature in the middle of the metallic plate along the reactor for countercurrent flow arrangement and step catalyst distribution (catalytic and homogeneous combustion).

[Color figure can be viewed in the online issue, which is available at wileyonlinelibrary.com.]

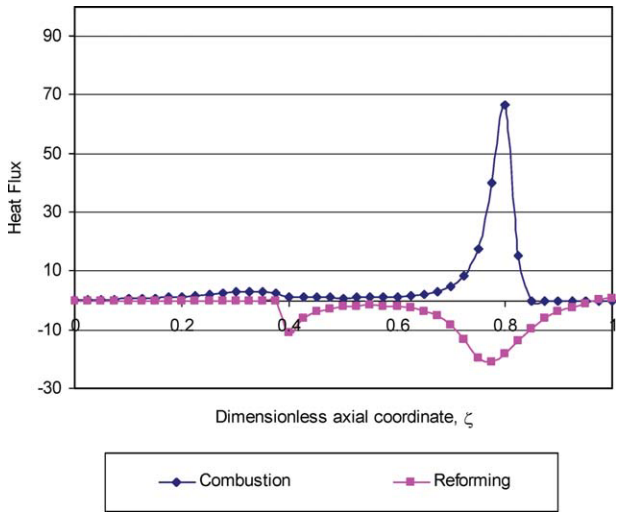

Figure 11. Evolution of exothermic and endothermic heat fluxes along the reactor for countercurrent flow arrangement and optimum step size catalyst distribution (catalytic and homogeneous combustion).

[Color figure can be viewed in the online issue, which is available at wileyonlinelibrary.com.]

the wall temperature reaches a value where homogeneous combustion could be initiated.[27] To assess the possibility of back propagation of the homogeneous combustion, a simplified reaction rate expression[27] for methane combustion in the gas phase was added to the gas-phase model in the combustion channel. The optimization problem (17) was solved for similar inlet conditions. The solution indicates an optimal geometry having a total reactor length of $L = 0.6$ m, $L_{\mathrm{ref}} = 0.225$ m, and $L_{\mathrm{comb}} = 0.104$ m. Figure 10 shows the spatial profile of the reforming and combustion methane conversions and the dimensionless temperature of the reactor wall. The exothermic and endothermic heat fluxes are presented in Figure 11. It can be seen that in this case the temperature peak is shifted toward the inlet of the combustion channel, whereas the peak temperature decreases to $T_{\max} = 1293$ K (significantly lower than $T_{\max} = 1484$ K in the catalytic combustion-only case). Moreover, the conversion at the outlet of the combustion channel increases to 91.7% because of the contribution of the homogenous reaction.

To assess the back propagation of the homogeneous combustion, the reaction rates of both the homogeneous and catalytic combustion reactions were scale related to their maximum value in the reactor and plotted as a function of the reactor length in Figure 12. Note that although the catalytic combustion is initiated at the dimensionless axial coordinate that corresponds to the beginning of the combustion catalyst layer, i.e., $\zeta = 0.8257$), homogeneous combustion begins at the very inlet of the combustion channel. However, the homogeneous contribution is small, as the methane conversion at the point where the fuel mixture reaches the combustion catalyst is only 5%. Note also that both the homogeneous and the catalytic reaction rates exhibit a maximum around the location of the wall temperature peak, and that the reactor is cooled down between the beginning of the reforming catalyst layer (dimensionless coordinate $\zeta = 0.375$) and the location of the temperature peak ($\zeta = 0.8$).

Increasing the combustion channel conversion

The results presented above indicate that in the optimized configurations the combustion conversion remains lower than the conversion in the reforming channel. It is likely that increasing the conversion in the combustion channel would entail using a leaner fuel mixture. This approach presents the disadvantage of a decreased fuel efficiency. In the present configuration, which relies on a stoichiometric air–methane mixture, the unspent fuel in the combustion channel exhaust

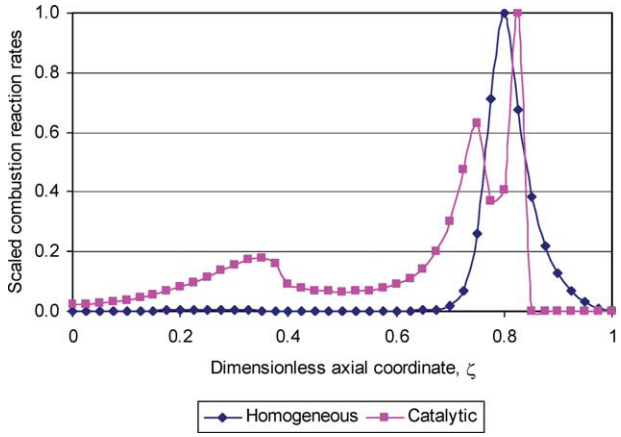

Figure 12. Scaled reaction rates for homogeneous and catalytic combustion along the reactor dimensionless axial coordinate.

[Color figure can be viewed in the online issue, which is available at wileyonlinelibrary.com.]

can be used to preheat the feed streams with only a minor efficiency penalty. Other potential avenues for improving fuel use include

- a multiple segmentation of the catalyst: intercalating several inactive portions in the combustion catalyst coating is likely to improve combustion conversion and allow for more flexibility in shaping the longitudinal temperature profile through optimization; note that, in the limit, catalyst segmentation is equivalent to the distributed fuel feed proposed by Kolios et al.[16]
- altering the choice of fuel and catalyst, and opting for a construction material with higher thermal conductivity.[14]

However, these modifications go beyond the scope of this work and will constitute the object of a future study.

Conclusions

This article investigated the influence of flow arrangement and catalyst distribution for the autothermal coupling of methane steam reforming and methane catalytic combustion in plate reactors. The reactor thermal behavior and performance for cocurrent and countercurrent have been simulated and compared. In the countercurrent case, a partial overlapping of the catalyst zones in adjacent exothermic and endothermic channels was shown to significantly increase reactor performance, while avoiding both severe hotspots and the extinction of the reactor. The effect of homogeneous combustion of the air–methane fuel mixture was investigated and was shown to have a significant impact on the optimal distribution of the catalyst. A rigorous optimization-based approach for determining the catalyst zone overlap that results in a maximum reactor conversion within specified temperature bounds was introduced. To our knowledge, no prior research has relied on this technique, and the present effort thus represents a significant step forward in this regard. Furthermore, the concept of using a dynamic model to obtain a steady-state optimal solution for the autothermal reactor was presented and demonstrated. The physics- and chemistry-based dynamic model modifications that were presented (e.g., time scale stretching, dynamic extensions) are considered to be of generic value for future studies concerning the simulation, design and optimization of stiff, and multiscale convection-diffusion-reacting flow systems.

Notation

c_p = heat capacity, J kg^{-1} K^{-1}
D_{eff} = effective diffusion coefficient, m^2 s^{-1}
D_G = molecular diffusion coefficient, m^2 s^{-1}
D_K = Knudsen diffusion coefficient, m^2 s^{-1}
Fo = Fourier number as defined by Eq. 13
H = reaction heat flux, W m^{-2}
k = gas thermal conductivity, W m^{-1} K^{-1} or reaction rate constant
K_e = equilibrium constant
L = reactor length, m
M = molecular weight, kg mol^{-1}
p_i = partial pressure, bar
P = total pressure, bar
r = reaction rate, mol kg$_{cat}^{-1}$ s^{-1}
r_{homog} = homogeneous combustion reaction rate, mol m^{-3}
R = half distance between the reactor plates, m
R_p = catalyst pore radius, m
R_g = universal gas constant, J mol^{-1} K^{-1}
T = temperature, K
u_z = axial mass velocity, m s^{-1}
x = transverse coordinate, m
X = conversion
z = axial coordinate, m

Greek letters

δ^{cat} = catalyst thickness, m
δ_s = wall thickness, m
ΔH = heat of reaction, J mol^{-1}
ε = catalyst porosity
λ_s = thermal conductivity of the solid wall, W m^{-1} K^{-1}
η = effectiveness factor
ν = stoichiometric coefficient
ρ = density, kg m^{-3}
τ = catalyst tortuosity
τ_d = transverse diffusion time as defined by Eq. 12
τ_s = local space time as defined by Eq. 11
ω = mass fraction
ζ = dimensionless axial coordinate

Subscripts

0 = inlet
i = chemical species
j = channel
k = reaction
s = solid wall
j = 1 Reforming
i = CH_4, H_2O, CO, CO_2, H_2, N_2
k = 1 methane steam reforming reaction
$CH_4 + H_2O \Leftrightarrow CO + 3H_2$
k = 2 water–gas shift reaction
$CO + H_2O \Leftrightarrow CO_2 + H_2$
k = 3 reverse methanation reaction
$CH_4 + 2H_2O \Leftrightarrow CO_2 + 4H_2$
j = 2 Combustion
i = CH_4, O_2, CO_2, H_2O, N_2
k = 1 methane catalytic combustion
$CH_4 + 2O_2 \Leftrightarrow CO_2 + 2H_2O$

Superscripts

g = gas phase
cat = catalyst layer

Literature Cited

1. *A Roadmap for the Twenty First Century*. Institution of Chemical Engineers, May 2007. www.icheme.org/AnnualReview2007a.pdf. Accessed on November 1, 2010.
2. Reay D, Ramshaw C, Harvey A. *Process Intensification: Engineering for Efficiency, Sustainability and Flexibility*. Amsterdam: Elsevier Ltd., 2008.
3. Dietrich TR. *Microchemical Engineering in Practice*. Hoboken, NJ: Wiley, 2009.
4. Hessel V, Renken A, Schouten JC, Yoshida J. *Micro Process Engineering: A Comprehensive Handbook*. Weinheim: Wiley VCH, 2009.
5. Venkataraman K, Redenius JM, Schmidt LD. Millisecond catalytic wall reactors: dehydrogenation of ethane. *Chem Eng Sci*. 2002;57:2335–2343.
6. Zanfir M, Gavriilidis A. Catalytic combustion assisted methane steam reforming in a catalytic plate reactor. *Chem Eng Sci*. 2003;58:3947–3960.
7. Tonkovich A, Perry S, Wang Y, Qiu D, LaPlante T, Rogers WA. Microchannel process technology for compact methane steam reforming. *Chem Eng Sci*. 2004;59:4819–4824.
8. Tonkovich A, Huhlmann D, Rogers A, McDaniel J, Fitzgerald S, Arora R, Yuschak T. Microchannel technology scale-up to commercial capacity. *Trans IChemE Part A, Chem Eng Res Des*. 2005;83:634–639.

9. Seris ELC, Abramowitz G, Johnston AM, Haynes BS. Scaleable, microstructured plant for steam reforming of methane. *Chem Eng J*. 2008;135S:S9–S16.
10. Velocys. http://www.velocys.com/technology/video. php, Accessed May 2010.
11. Zanfir M, Gavriilidis A. Influence of flow arrangement in catalytic plate reactors for methane steam reforming. *Trans IChemE, Part A, Chem Eng Res Des*. 2004;82:252–258.
12. Deshmukh SR, Vlachos DG. Effect of flow configuration on the operation of coupled combustor/reformer microdevices for hydrogen production. *Chem Eng Sci*. 2005;60:5718–5728.
13. Baldea M, Daoutidis P. Dynamics and control of autothermal reactors for the production of hydrogen. *Chem Eng Sci*. 2007;62:3218–3230.
14. Stefanidis GD, Vlachos DG. Intensification of steam reforming of natural gas: choosing combustible fuel and reforming catalyst. *Chem Eng Sci*. 2010;65:398–404.
15. Vaccaro S, Malangone L, Ciambelli P. Modelling of a catalytic micro-reactor coupling endothermic methane reforming and combustion. *Int J Chem React Eng*. 2010;8:A51.
16. Kolios G, Gritsch A, Morillo A, Tuttlies U, Bernnat J, Opferkuch F, Eigenberger G. Heat-integrated reactor concepts for catalytic reforming and automotive exhaust purification. *Appl Catal B: Environ*. 2007;70:16–30.
17. Baratti R, Tronci S, Zanfir M, Gavriilidis A. Optimal catalyst distribution in catalytic plate reactors. *Int J Chem React Eng*. 2003;A58. www.bepress.com/ijcre/vol1/A58. Accessed on November 1, 2010.
18. Ramaswamy RC, Ramachandran PA, Dudukovic MP. Recuperative coupling of exothermic and endothermic reactions. *Chem Eng Sci*. 2006;61:459–472.
19. Elnashaie SSEH, Adris AM, Al-Ubaid AS, Soliman MA. On the non-monotonic behaviour of methane-steam reforming kinetics. *Chem Eng Sci*. 1990;45:491–501.
20. Xu J, Froment GF. Methane steam reforming, methanation and water-gas shift. I. Intrinsic kinetics. *AIChE J*. 1989;35:88–96.
21. Yao YFY. Oxidation of alkanes over noble metal catalysts. *Ind Eng Chem Prod Res Dev*. 1980;19:293–298.
22. Trimm DL, Lam CW. The combustion of methane on platinum-alumina fibre catalysts. I. Kinetics and mechanism. *Chem Eng Sci*. 1980;35:1405–1413.
23. Cullis CF, Willatt BM. Oxidation of methane over supported precious-metal catalysts. *J Catal*. 1983;83:267–285.
24. Lee JH, Trimm DL. Catalytic combustion of methane. *Fuel Proc Tech*. 1995;42:339–359.
25. Aryafar M, Zaera F. Kinetic study of the catalytic oxidation of alkanes over nickel, palladium and platinum foils. *Catal Lett*. 1997;48:173–183.
26. Hodnett BK. *Heterogeneous* Catalytic Oxidation, Fundamental and Technological Aspects of the Selective and Total Oxidation of Organic Compounds. New York: Wiley, 2000.
27. Frauhammer J. Ein neues Gegenstromreaktorkonzept für endotherme Hochtemperaturreaktionen, Dissertation, Institut für Chemische Verfahrenstechnik, Fortschr.-Ber. VDI Reihe 3 Nr. 792. Düsseldorf: VDI Verlag, 2003.
28. Bird BR, Steward WE, Lightfoot EN. *Transport Phenomena*. New York: Wiley, 1960.
29. Hayes RE, Kolaczkowski ST. *Introduction to Catalytic Combustion*. Amsterdam: Gordon and Breach Science Publisher, 1997.
30. Oh M, Pantelides CC. A modelling and simulation language for combined lumped and distributed parameters systems. *Comput Chem Eng*. 1996;20:611–633. www.psentrerprise.com/gproms. Accessed on November 1, 2010.
31. Finlayson B. *Non-Linear Analysis in Chemical Engineering*. New York: McGraw Hill, 1980.
32. Cellier F, Koffman E. *Continuous System Simulation*. New York, NY: Springer Verlag, 2006.
33. Boyd S, Vandenberghe L. *Convex Optimization*. Cambridge: Cambridge University Press, 2004.
34. Kokotovic PV, Khalil HK, O'reilly J. *Singular Perturbation Methods in Control: Analysis and Design*. Philadelphia: Society for Industrial Mathematics, 1999.
35. Baldea M, Jibb, RJ, Cano A, Ramos A. A framework for dynamic modeling and optimization of multi-stream plate-fin heat exchangers, *AIChE Annual Meeting*, Nashville, TN, 2009.
36. Kolios G, Frauhammer J, Eigenberger G. Autothermal fixed-bed reactor concepts. *Chem Eng Sci*. 2000;55:5945–5967.

Manuscript received May 28, 2010, and revision received Sept. 29, 2010.